



Power Electronic Systems  
Laboratory

© 2012 IEEE

Proceedings of the 7th IEEE International Power Electronics and Motion Control Conference (ECCE Asia 2012), Harbin, China,  
June 2-5, 2012

## **Analysis of Rotor Shell Losses in a Magnetically Levitated Homopolar Hollow-Shaft Permanent Magnet Synchronous Motor**

C. Zingerli,  
T. Nussbaumer,  
J. W. Kolar

This material is published in order to provide access to research results of the Power Electronic Systems Laboratory / D-ITET / ETH Zurich. Internal or personal use of this material is permitted. However, permission to reprint/republish this material for advertising or promotional purposes or for creating new collective works for resale or redistribution must be obtained from the copyright holder. By choosing to view this document, you agree to all provisions of the copyright laws protecting it.



Eidgenössische Technische Hochschule Zürich  
Swiss Federal Institute of Technology Zurich

# Analysis of Rotor Shell Losses in a Magnetically Levitated Homopolar Hollow-Shaft Permanent Magnet Synchronous Motor

Claudius M. Zingerli and Johann W. Kolar  
Power Electronic Systems Laboratory  
ETH Zurich  
8092 Zurich, Switzerland  
Email: zingerli@lem.ee.ethz.ch

Thomas Nussbaumer  
Levitronix GmbH  
Technoparkstr. 1  
8005 Zurich, Switzerland  
Email: nussbaumer@levitronix.com

**Abstract**—This paper analyzes challenges that arise when the rotational speed in magnetically levitated hollow-shaft PMSMs is increased. Going to higher speeds highlights the advantages of such machines as being contact and contamination free, but leads to considerably higher losses. We propose a model and supply experimental data and simulations to subdivide losses into different categories with regard to specific optimizations. We particularly focus on the high rotor shell eddy current losses specific for this machine.

**Index Terms**—Magnetic levitation, Modeling, Eddy currents, Permanent magnet machines, Bearingless drives

## I. MOTIVATION

Replacing mechanical bearings by magnetic bearings widens the area of applications of an electrical drive in semiconductor manufacturing, biological or chemical processes because of the lack of contamination, lower shear stresses and simple hermetical isolation. This results in increasing reproducibility, cleanness, controllability of the processes and therefore higher output.

Another factor that influences the output of e.g. cleaning, particle coating or separation processes is speed. The aim of this paper is to examine the suitability of magnetically levitated hollow-shaft motors presented in [1] at higher speeds, an issue that - until now - has not been studied in detail.

The magnetically levitated hollow-shaft motor design is closely related to the bearingless motor design, where the magnetic bearing and drive share the same magnetic circuit. In the design we propose, they share the same magnetic circuit on the rotor, whereas they are separated on the stator side. This approach maintains the advantages of a hollow and flat rotor, i.e. a minimal construction height, which allows for an installation in very limited spaces or inside a straight pipe. The separation of the magnetic circuits of bearing and drive on the stator side allows for specific optimizations to achieve minimal losses as shown in [2].

Initially, losses were mainly to be expected in the rotor iron, the drive core and the copper windings, but experiments have indicated a further significant source of losses in the rotor shell. In transient 3D FEM-based simulations carried out after this discovery, it was possible to model shell losses very well.

For this reason, this publication mainly focuses on the analysis of the losses generated in the rotor shell. While all magnetic parts can be made of laminated steel or plasticized compounds, the rotor mantle has to be made of rigid material to withstand the strong centrifugal forces of the rotor magnets. Furthermore the rotor shell must be made of electrically well conductive material for the position sensors of the active magnetic bearing to work. As the rotor shell is in the path of the magnetic fields of the bearing and drive, eddy current losses are unavoidable under such circumstances.

In the following sections, first we will first give a short introduction into the magnetically levitated homopolar motor, followed by a more detailed description of the experimental system. Subsequently, loss modeling and loss analysis are covered using data from experiments as well as from simulations. Ultimately, conclusions are drawn, including directions for further optimizations.

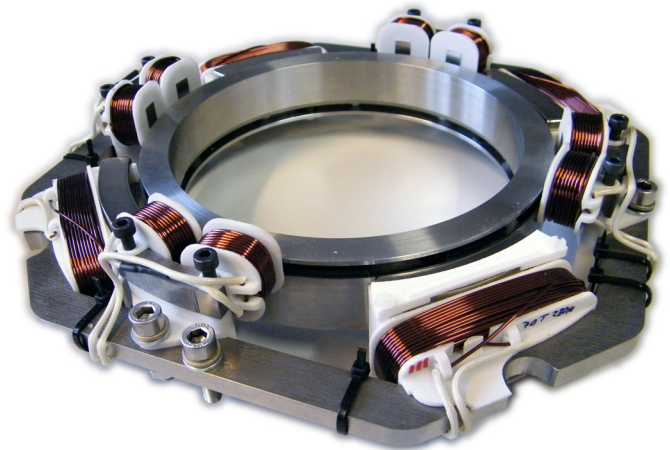


Figure 1: Prototype of a high-speed magnetically levitated hollow-shaft PMSM.

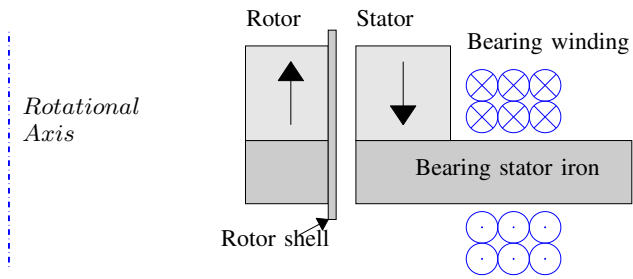


Figure 2: Cut through the MHM topology. The rotor and bearing stator iron lamination are displayed in dark gray. The opposite magnetized rotor and stator permanent magnets, shown in light gray, attract each other stabilizing tilting and axial position. With the bearing winding (illustrated in blue) the flux density in the air gap can be controlled resulting in a radial force.

## II. CHOICE OF TOPOLOGY

Several different topologies of disc shaped magnetically levitated motor concepts have already been analyzed and successfully implemented in the past (p.e. [3–5]). In [6], the magnetically levitated homopolar motor (MHM) shows the lowest losses of the four topologies studied at a speed of 1500 rpm. Therefore the MHM topology was chosen to be analyzed in this study. Even if we aim at speeds between 5 krpm and 12 krpm, it is plausible that this choice is optimal for similar dimensions at higher speeds as well, given that the in all cases dominating eddy current and hysteresis losses increase with the frequency at least linearly.

The MHM topology - as shown in Figures 2 and 3 - consists of a flat rotor with discrete axially magnetized permanent magnets on top of a ferromagnetic ring. These magnets act together with the magnets on the bearing stator as a passive magnetic bearing that stabilizes the axial and the two tilting directions. An additional biaxial active magnetic bearing consisting of windings around the bearing poles, controls the radial position of the rotor.

By setting the width of a bearing pole  $b_w$  (Figure 3) as wide as an even multiple of the rotor (drive) pole width, the dependence of both reluctance on the rotor angle and clogging torque can be minimized<sup>1</sup>. Thanks to this homopolar design, the influence of the rotor field on the bearing is small, compared to other types of bearingless drives. This becomes even more interesting at higher speeds. Only the - compared to the bearing stator - relatively small volume of the drive stator core shows alternating flux densities from what we would expect low losses.

To generate a torque, a rotating magnetic field is created above the rotor using multiple segments as described in [2].

<sup>1</sup>This approach neglects 3D stray-flux paths, but FEM-based magnetostatic simulations as well as measurements have shown that the clogging torque due to the bearing is below 3% of the drive torque.

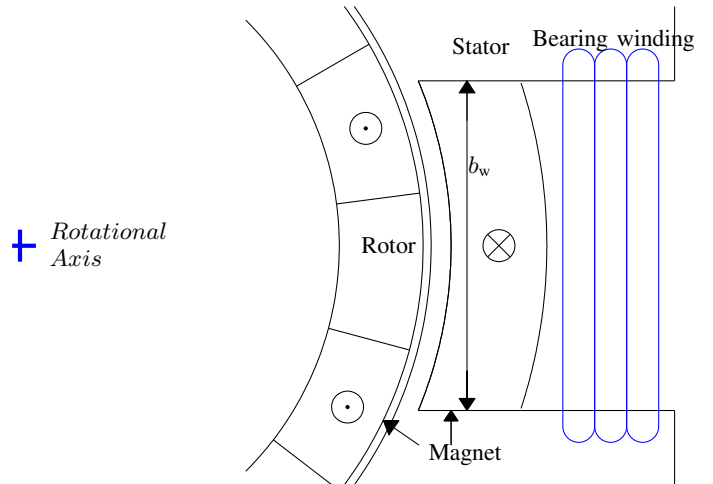


Figure 3: Top view of the MHM topology showing one bearing pole. The drive stator consists of several C or E-shaped cores next to the bearing pole.

## III. EXPERIMENTAL SYSTEM

In order to analyze the losses of a magnetically levitated hollow-shaft motor, a prototype has been developed as shown in Figure 1. Key parameters are given in Table I.

For the experiment, the rotor diameter was chosen to fit standard industrial DN150 piping with minimal resistance to the passing process fluid. From this size, most other geometric dimensions can be derived.

The active magnetic bearing consists of two orthogonal pole pairs (x and y) what allows the use of two independent controllers. A practical lower limit of 10 drive pole pairs appears convenient in view of restrictions like homopolar pole arrangement, planar mounting of the drive and bearing stator, and also because position sensors have to be fitted in. On the stator side, due to space limitations, only four pole pairs of the drive were implemented in a two-phase configuration.

The rotor is enclosed by a shell made of non-magnetic stainless steel to isolate the internal components from the environment as well as to hold them together (Figure 4).



Figure 4: Open rotor of the prototype system. Shown is the ferromagnetic ring with the rotor magnets on top, enclosed by the rotor shell made of stainless steel.

Table I: Key parameters of the experimental system

Mechanic air gap $\delta_{\text{mech}}$	1 mm
Rotor inner diameter $d_i$	130 mm
Rotor outer diameter $d_o$	164 mm
Rotor mass $m_r$	0.86 kg
Rotor height $h_r$	28 mm
Rotor design speed $n_{\text{max}}$	12000 1/min
Rotor nominal speed $n$	7000 1/min
Air gap $\delta_{\text{mag}}$	2.5 mm
Drive phases $p_{\text{DRV}}$	2
Drive poles $n_{\text{p(DRV)}}$	20
Active bearing axes $p_{\text{BNG}}$	2
Bearing poles $n_{\text{p(BNG)}}$	4
Passive axial stiffness $k_z$	33.5 N/mm
Passive radial stiffness $k_x$	-21.7 N/mm
Current-Force constant $k_i$	-88 N/kA/turn
Motor speed constant $k_m$	2.74 mVrms · min

#### IV. LOSS MEASUREMENT AND ANALYSIS

Even though an optimized bearing geometry was used, considerable losses were measured in the prototype system. In order to be able to minimize these losses, they have to be analyzed and split into different source terms. Figure 5 shows the model used to analyze the power flow displayed as a Sankey diagram (named after Cpt R. Sankey).

##### A. Input power

The controller losses  $P_{\text{(ctr)}}$  can be calculated from the difference of the input power  $P_{\text{in}}$ , the bearing effective power  $\Re(S_{\text{bng}})$  and the drive power  $P_{\text{drv}}$ .

##### B. Copper losses

The bearing effective power was assumed to cause purely ohmic losses. An analysis of the bearing impedance did not show significant AC losses at the frequencies present in the system<sup>2</sup>, therefore

$$\Re(S_{\text{bng}}) = P_{\text{l(bng,cu)}} = \sum_{\forall k} R_{\text{bng}} \cdot I_{\text{bng},k}^2 \quad (1)$$

The same applies to copper losses of the drive

$$P_{\text{l(drv,cu)}} = \sum_{\forall k} R_{\text{drv}} \cdot I_{\text{drv},k}^2 \quad (2)$$

Due to the homopolar bearing design and the permanent magnet-based biasing, under normal conditions, the current in the bearing is very small ( $< 1$  Arms). If the rotor is not well balanced, the current rises remarkably. Further, if the sizes of the rotor and stator magnets are not matched, the rotor starts

<sup>2</sup>At a speed of  $n = 10$  krpm, the resistance  $R_{\text{bng}}$  increases by 5%.

oscillating what results in high currents in the bearing trying to balance the rotor.

In the prototype system, the bearing and drive resistances are  $R_{\text{bng}} = 0.82 \Omega$  and  $R_{\text{drv}} = 0.50 \Omega$ , causing very minor copper losses of  $P_{\text{l(bng,cu)}} = 1.16$  W and  $P_{\text{l(drv,cu)}} = 8.76$  W at a speed of  $n = 7000$  rpm at an input power of  $P_{\text{in}} = 131$  W.

##### C. Rotor power

The power fed into the rotor can be calculated from the drive currents  $I_{\text{drv},k}$ , the rotor speed  $n$  and the motor constant  $k_m$  as

$$P_{\text{rot}} = n \cdot k_m \cdot \sum_{\forall k} I_{\text{drv},k} \quad (3)$$

The moving rotor is affected by fluid friction losses. Assuming these are limited to the gap  $h$  between the outer rotor surface  $A_{\text{r,out}}$  and the casing and that they obey newtonian fluid friction laws (Dynamic viscosity  $\mu = \text{const}$ ), the power

$$F_r = \frac{1}{2} \mu \cdot A_{\text{r,out}} \cdot \omega \cdot d_o / h \quad (4)$$

$$T_{\text{air}} = F_r \cdot \frac{d_o}{2} \quad (5)$$

$$\begin{aligned} P_{\text{fluid}} &= T_{\text{air}} \cdot \omega \\ &= \frac{1}{4} \mu \cdot A_{\text{r,out}} \cdot \omega^2 \cdot d_o^2 \end{aligned} \quad (6)$$

is lost (Rotor outer diameter  $d_o$  and speed  $\omega$  in  $[\omega] = \text{rad/s}$ ). The fluid friction in gases is small and the air gap of the prototype is wide, thus playing a minor role in the total rotor losses. Dominant are eddy current losses as will be discussed in the following section.

##### D. Eddy current losses

The difference between the remaining rotor power  $P_{\text{rot}} - P_{\text{fluid}}$  and the machine output power  $P_{\text{out}}$  is the power lost because of eddy currents  $P_{\text{eddy}}$  in conductors and hysteresis losses in the magnetic materials. We distinguish between two mechanisms that create eddy current losses: losses on the drive and bearing stator because of the rotor field and those occurring on the rotor due to the stator field.

As the bearing stator geometry has been designed for a minimal flux amplitude and the drive stator field rotates synchronously with the rotor, the majority of eddy current losses are expected on the rotor. The measured stator temperature rise was minimal and can be explained alone by ohmic heating from the windings. Eddy current losses on the rotor

$$P_{\text{eddy}} = P_{\text{ed(iron)}} + P_{\text{ed(magnet)}} + P_{\text{ed(shell)}} \quad (7)$$

consist of losses in the back iron ring, the rotor magnets and the rotor shell.

##### E. Losses in the rotor shell $P_{\text{ed(shell)}}$

As the rotor shell is the mechanically highest loaded part, a detailed analysis of the losses in the rotor shell is essential. A thicker rotor shell is more rigid but generally implies higher losses. Higher losses generate more heat what again weakens the shell material. The use of a less conductive or thinner shell

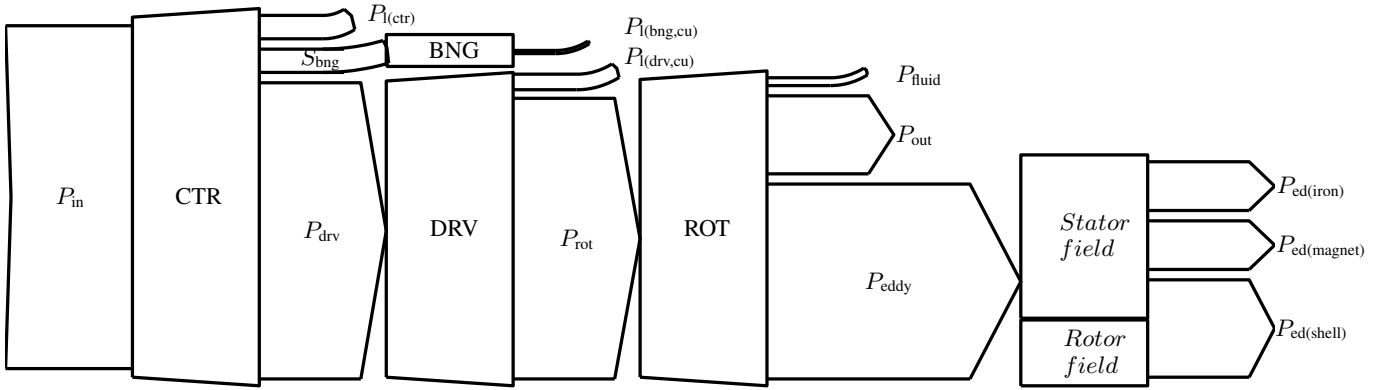


Figure 5: Model of the different flows of power in the drive system. Input power  $P_{in}$  is fed into the controller CTR that supplies the bearing BNG and drive DRV. The majority of the drive power  $P_{drv}$  goes through the air gap into the rotor ROT. Using this power, the rotor does work with  $P_{out}$ . Due to the strong coupling of the bearing and drive magnetic fields, a significant part  $P_{eddy}$  of the rotor power  $P_{rot}$  is transformed into heat because of stator and rotor field induced eddy currents occasioning a breaking torque.

Table II: Skin depth in rotor shell. Full penetration of the magnetic field through the 1 mm thick rotor shell can be assumed at all rotational speeds. The number of rotor poles  $n_{p(DRV)}$  is always 20. (Data adapted from [7])

Material	Resistivity $\rho_k$ at $T = 60^\circ\text{C}$	Skin depth $\delta$ at speed $n$		
		4 krpm	7 krpm	10 krpm
Copper	19.4 n $\Omega \cdot \text{m}$	6.8 mm	5.1 mm	4.3 mm
Aluminium	32.6 n $\Omega \cdot \text{m}$	8.8 mm	6.7 mm	5.6 mm
Steel 1.304	716 n $\Omega \cdot \text{m}$	41.4 mm	31.3 mm	26.2 mm

makes position sensing more difficult what affects bearing stability. To counter both of these effects, thick metallic shells are preferred what leads to - once more - high eddy current losses.

At the frequencies of the magnetic field on the rotor, the thickness of the shell  $s_m$  is well below the skin depth  $\delta$  (Table II). Therefore full penetration of the magnetic field through the shell can be assumed. Using Faraday's law of induction, losses in the rotor shell can be estimated as

$$P_{ed(shell)} = V_{EMF(shell)}^2 \cdot G_{shell} = \left( \frac{\partial B}{\partial t} \right)^2 \cdot G_{shell} \propto c_0 \cdot \omega^2 \cdot G_{shell} \quad (8)$$

using the constant  $c_0$  to model the flux density change in the shell,  $\omega$  as the angular velocity and  $G_{shell}$  the electric conductance of the shell.

To analyze and model losses generated in the rotor shell, experiments with layers of metal foil wound around the shell using different thicknesses  $d_k$  and materials  $k$  were conducted.

Assuming eddy current losses in all parts of the rotor in

equation (7) to be proportional to  $\omega^2$  as

$$P_{eddy} = \omega^2 (c_{iron} + c_{magnet} + c_0 \cdot G_{shell}) \quad (9)$$

using the two constants  $c_{iron}$  and  $c_{magnet}$  to model the losses in the rotor back iron and magnets as well as the shell losses in the layered shell by replacing the conductivity

$$G_{shell} = \sum_{\forall k} \frac{d_k}{\rho_k} \quad (10)$$

for the shell layers  $k$ , the shell losses

$$P_{ed(shell)} = c_0 \cdot \omega^2 \cdot \left( \frac{d_{steel}}{\rho_{steel}} + \frac{d_{cu}}{\rho_{steel}} + \frac{d_{al}}{\rho_{steel}} \right) \quad (11)$$

can be extracted from the total rotor eddy current losses through variation of the thicknesses of the shell materials. This was done experimentally by attaching multiple layers of copper or aluminium ribbon around the shell made of stainless steel to achieve a total shell thickness of  $d_{steel} + d_{cu} + d_{al}$ .

This method allows for an estimation of the potential reduction of losses by extrapolation to an ideal shell thickness of zero.

In order to find the constants  $c_0$  and  $c_{iron} + c_{magnet}$ , measurements of the rotor losses (calculated from the drive currents, as shown in section IV-C) are done at different speeds

$$n = \{1000, 2000, \dots, 7000\} \text{ min}^{-1}$$

and with different ribbons

$$\begin{aligned} d_{steel} &= 1 \text{ mm} \quad , \\ d_{cu} &= \{0, 35, 70, 105, 140\} \mu\text{m} \text{ and} \\ d_{al} &= \{0, 48, 96, 144\} \mu\text{m} \quad . \end{aligned}$$

The constants  $c_{iron} + c_{magnet}$  are added to  $c_1$ . Using a linear regression over the measured losses, the parameters  $c_0 = 59.5 \text{ n}\Omega \cdot \text{W} \cdot \text{s}^2$  and  $c_1 = 125.8 \mu\text{W} \cdot \text{s}^2$  were found. The results are shown in Figure 6. By reducing the thickness of

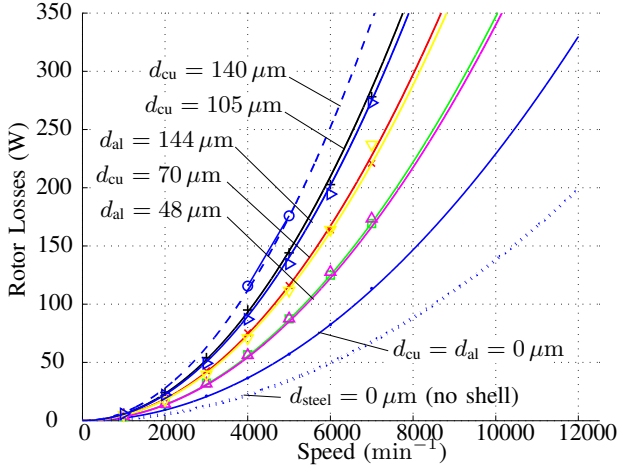


Figure 6: Comparison of measured losses (Markers) and model based loss distribution (Lines). The lowest, dotted line shows the theoretical rotor losses without shell losses using the model described in section IV. At  $n = 7000 \text{ min}^{-1}$ ,  $P_{\text{ed(shell)}} = 45.6 \text{ W}$  are lost in the rotor shell.

the rotor shell to zero, the losses in the rotor back iron and magnets remain as

$$P_{\text{ed(iron)}} + P_{\text{ed(mag)}} = c_1 \cdot \omega^2 \quad (12)$$

$$= \begin{cases} 12.4 \text{ W} & (n = 3000 \text{ min}^{-1}) \\ 49.7 \text{ W} & (n = 6000 \text{ min}^{-1}) \\ 112 \text{ W} & (n = 9000 \text{ min}^{-1}) \\ 198 \text{ W} & (n = 12000 \text{ min}^{-1}) \end{cases},$$

with shell losses in the  $d_{\text{steel}} = 1 \text{ mm}$  thick steel shell of

$$P_{\text{ed(shell)}} = c_0 \cdot \omega^2 \cdot d_{\text{steel}} / \rho_{\text{steel}} \quad (13)$$

$$= \begin{cases} 8.20 \text{ W} & (n = 3000 \text{ min}^{-1}) \\ 32.8 \text{ W} & (n = 6000 \text{ min}^{-1}) \\ 73.8 \text{ W} & (n = 9000 \text{ min}^{-1}) \\ 131 \text{ W} & (n = 12000 \text{ min}^{-1}) \end{cases}.$$

## V. SIMULATION

As the MHM presents a relatively flat topology, the magnetic fields above and below the machine play an important role. For this reason, all simulations were done in 3D with the finite element method (FEM). In the initial design phase, using magnetostatic simulations, feasibility was studied with regards to startability and controllability, while applying procedures published in [2, 5].

Later on, the experienced rotor shell losses were studied using transient moving-mesh FEM-based simulations as shown in Figures 7, 8 and 9.

While the magnetostatic simulations took about 30' per geometry on a 16-core 2.4 GHz PC, a transient simulation at a fixed speed took about 4h until the loss calculation converged. As the losses partly depend on the rotor angle, the simulated time was chosen so that the rotor turns 90 degrees independent

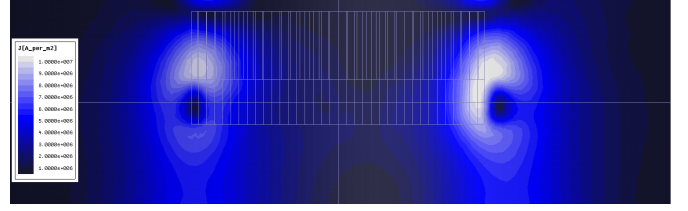


Figure 7: Simulated current density distribution in the rotor shell rotating at a speed of  $n = 12000 \text{ min}^{-1}$  from the left to the right as seen radially from a bearing pole. (Linear color scale from  $1 \text{ A/mm}^2$  to  $10 \text{ A/mm}^2$ .)

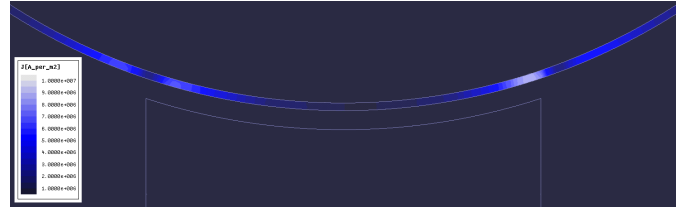


Figure 8: Same as Figure 7, but seen from the top of a bearing pole, at a level centered to the iron lamination.

of its speed (what equals 900 degrees electrical). Iron laminations were modeled as electrically isolating and magnetically linear materials in order to speed up the simulation.

The rotor shell losses displayed in Figure 9 match within 15% to the modeled and measured losses shown in Figure 6. The current densities in the rotor shell (Figures 7 and 8) peak as expected close to the bearing poles. A further result of the transient simulation is that the breaking torque (blue lines in Figure 9) changes significantly with the rotor angle.

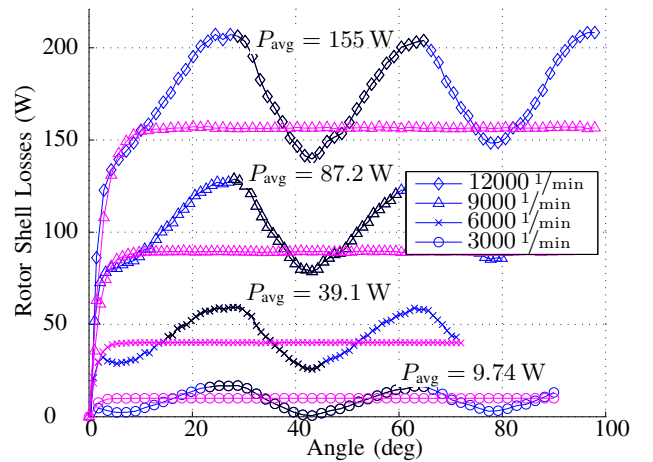


Figure 9: Simulated rotor shell losses at different speeds. The losses calculated by integrating the current density (purple) stay constant, while the losses calculated from the breaking torque (blue) vary with the rotor angle as the rotor magnets pass by the bearing stator poles.

## VI. CONCLUSIONS

The MHM topology is suitable at higher speeds in case the rotor shell losses are reduced. Even then, the bearing itself does not consume much power, but because of permanent magnet biasing and variable reluctance, it induces losses in the rotor resulting in a breaking torque. These losses are especially pronounced in the rotor shell. A reducing of the bearing bias will produce smaller rotor losses but also lower stiffness - especially on the purely passively stabilized tilting axes. Therefore, future research has to find an optimum between losses and bearing stability.

A different approach would be to use a rotor position sensor that does not depend on conducting materials or sensorless control permitting the application of isolating rotor shells.

It has further been shown that it is possible to model the rotor shell losses using 3D transient FEM-based simulations with useful accuracy, what allows a better prediction of losses during the initial design. On the one hand, similar problems can be expected in other machines at higher speeds, where a conducting rotor or stator shell is moved relative to a magnetic field like in many bearingless drives or magnetic bearings - and, on the other hand, they can be assessed using the afore presented methods.

## REFERENCES

- [1] T. Schneeberger, T. Nussbaumer, and J. W. Kolar, "Magnetically levitated homopolar hollow-shaft motor," *IEEE/ASME Trans. Mechatronics*, vol. 15, no. 1, pp. 97–107, 2010.
- [2] T. Schneeberger, "Integriertes magnetisches lager- und antriebssystem fuer halbleiterwafer," Ph.D. dissertation, ETH Zurich, 2008.
- [3] M. Ooshima, A. Chiba, T. Fukao, and M. A. Rahman, "Design and analysis of permanent magnet-type bearingless motors," *IEEE Trans. Ind. Electron.*, vol. 43, no. 2, pp. 292–299, 1996.
- [4] S. Silber, W. Amrhein, P. Bosch, R. Schob, and N. Barletta, "Design aspects of bearingless slice motors," *IEEE/ASME Trans. Mechatronics*, vol. 10, no. 6, pp. 611–617, 2005.
- [5] P. Karutz, T. Nussbaumer, W. Gruber, and J. W. Kolar, "Novel magnetically levitated two-level motor," *IEEE/ASME Trans. Mechatronics*, vol. 13, pp. 658–668, dec. 2008.
- [6] T. Nussbaumer, P. Karutz, F. Zurcher, and J. W. Kolar, "Magnetically levitated slice motors—an overview," *IEEE Trans. Ind. Appl.*, vol. 47, no. 2, pp. 754–766, 2011.
- [7] CSNDT, "Conductivity and resistivity values for misc. materials," March 2002. [Online]. Available: <http://www.ndt-ed.org/GeneralResources/>